CO6-1

Structural Study for Higher Ordered Chromatin

H. Kurumizaka and M. Sugiyama[1]
Faculty of Science and Engineering, Waseda University
[1]Research Reactor Institute, Kyoto University

INTRODUCTION: In eukaryotic cells, genomic DNA is compacted and accommodated in the nucleus. To do so, the DNA must be formed a highly compacted structure, called chromatin. The fundamental unit of chromatin is the nucleosome, in which histones H2A, H2B, H3, and H4 are protein components. Two of each of histones form an octamer, containing two copies of each H2A-H2B and H3-H4 dimers, and approximately 150 base pairs of DNA are tightly bound to this histone core [1].

In cells, nucleosomes are extremely stable, but they have to be dynamic to promote DNA functions, such as repair, replication, recombination, and transcription [2,3]. Especially, nucleosomes are slide and reposition along genomic DNA by spontaneous and/or enzymatic remodeling processes [4,5]. It has been known that the nucleosome remodeling is an essential process for transcription, DNA repair, and replication. Intriguingly, a nucleosome repositioned by the remodeling process collides with a neighboring nucleosome [6,7]. This nucleosome collision forms the intermediate structure, called "overlapping dinucleosome" [6,7]. The overlapping dinucleosome may also be formed by another mechanism such as a DNA-sequence–directed nucleosome positioning, if two positioning DNA sequences for nucleosomes are located in close proximity enough to form the overlapping dinucleosome on the genomic DNA [6,7]. However, the structure of the over- lapping dinucleosome has remained elusive.

We previously determined the crystal structure of the overlapping dinucleosome. In the overlapping dinucleosome structure, In the overlapping dinucleosome structure, two nucleosomes are collided, and one H2A-H2B dimer is released. Consequently, the canonical octasome nucleosome containing a histone octamer and the unusual hexasome containing a histone hexamer are associated with new interactions between two nucleosomes [8]. This finding suggested that, in the overlapping dinucleosome, the octasome and hexasome moieties may dynamic interact each other. However, it has not been reported the dynamic property of the overlapping dinucleosome, so far. Therefore, in the present study, we reconstitute the overlapping dinucleosome in vitro, and studied its dynamic property in solution by small angle X-ray scattering (SAXS) method.

EXPERIMENTS: Human histones H2A, H2B, H3, and H4 were bacterially produced, and were purified near homogeneity. The 250 base-pair DNA was also produced in bacterial cells, and was purified. Then, the overlapping dinucleosome was reconstituted by a salt-dialysis method.

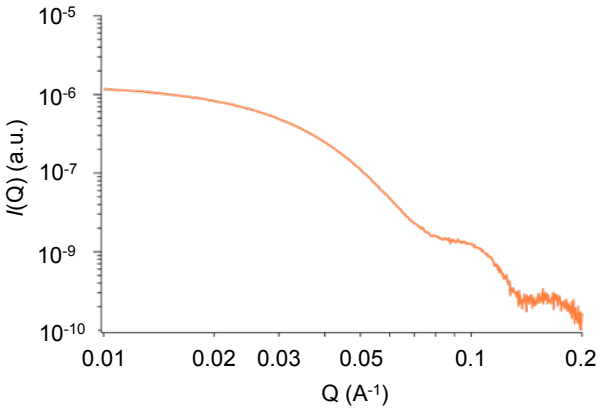

Fig. 1. SAXS profiles of the overlapping dinucleosome

The reconstituted overlapping dinucleosome was further purified by a native polyacrylamide gel electrophoresis. The purified overlapping dinucleosome samples were concentrated with a cartridge filter, and the debris was removed by centrifugation. We then performed the SAXS experiments.

RESULTS: As shown in Fig. 1, the SAXS curve was obtained, and solution parameters of the overlapping dinucleosome structure were estimated. A low resolution solution structure of the overlapping dinucleosome was obtained by Dummy atom modeling. The comparative study between solution structure and the X-ray structure of the overlapping dinucleosomes are underway.

REFERENCES:

[1] K. Luger *et al.*, Crystal structure of the nucleosome core particle at 2.8 A resolution. *Nature*., **389** (1997) 251-260.

[2] B. Li *et al.* The role of chromatin during transcription. *Cell*., **128** (2007) 707-719.

[3] R. Kornberg *et al*. Twenty-five years of the nucleosome, fundamental particle of the eukaryote chromosome. *Cell*., **98** (1999) 285-294.

[4] M. Bruno *et al.*, Histone H2A/H2B dimer exchange by ATP-dependent chromatin remodeling activities. *Mol. Cell.*, **12** (2003) 1599–1606.

[5] P. Becker *et al.*, ATP-dependent nucleosome remodeling. *Annu Rev Biochem.,* **71** (2002) 247-273.

[6] N. Ulyanova *et al.*, Human SWI/SNF gener-ates abundant, structurally altered dinucleo-somes on polynucleosomal templates. *Mol Cell Biol.,* **25** (2005) 11156-11570.

[7] M. Engeholm *et al.*, Nucleosomes can invade DNA territories occupied by their neighbors. *Nat Struct Mol Biol.,* **16** (2009) 151-158.

[8] D. Kato *et al*., Crystal structure of the overlapping dinucleosome composed of hexasome and octasome. *Science.,* **356** (2017) 205-208.

CO6-2 Structural Study for the *S. pombe* Overlapping Dinucleosome

M. Koyama, R. Inoue[1], W. Nagakura, M. Sugiyama[1] and H. Kurumizaka

Division of Advanced Science and Engineering, Waseda University

[1]*Research Reactor Institute, Kyoto University*

INTRODUCTION:

In the eukaryotic nucleus, genomic DNA binds to histone proteins to form the chromatin structure. The fundamental unit of the chromatin structure is the nucleosome, in which about 150-base-pairs of DNA are wrapped around the histone octamer, containing two molecules of each of four core histones (H2A, H2B, H3, and H4) [1, 2]. Although the nucleosome is the major structural unit of chromatin, it is also known that the structures different from the conventional nucleosome can be formed under specific conditions. For example, when four core histones are mixed with a 250-base-pair DNA fragment, which is longer than the mono-nucleosomal DNA (150-base-pairs) but shorter than the di-nucleosomal DNA (300-base-pairs), the structure called 'overlapping dinucleosome' is formed [3]. The overlapping dinucleosome is the structure, in which the DNA is wrapped continuously around the histone octamer (containing two H2A-H2B dimers and two H3-H4 dimers) and hexamer (containing one H2A-H2B dimer and two H3-H4 dimers) [3]. It is assumed that these structures such as overlapping dinucleosome are also formed on the genomic DNA *in vivo*, playing key roles in regulating the genome function.

The fission yeast *S. pombe* is a unicellular eukaryote that has a simple genome but shares many characteristics of the chromatin organization with higher eukaryotes such as human. Furthermore, *S. pombe* is readily manipulated in the laboratory. Therefore, *S. pombe* is useful as a model organism to study chromatin structure and function. Recently, we established a system to purify *S. pombe* four canonical histones, and reconstituted the *S. pombe* nucleosome *in vitro* [4]. Furthermore, the biochemical and biophysical assays revealed that the *S. pombe* nucleosome possesses unstable nature, and its DNA ends are frexible, as compared to the canonical human nucleosome [4]. In this study, we reconstituted the *S. pombe* overlapping dinucleosome *in vitro*, and measured its small angle X-ray scattering profiles to analyze its structural properties.

EXPERIMENTS:

The *S. pombe* overlapping dinucleosome was reconstituted *in vitro*, by mixing a 250-base-pair DNA fragment with *S. pombe* four canonical core histones (SpH2A, SpH2B, SpH3, SpH4). The reconstituted overlapping dinucleosome was further purified by polyacrylamide gel electrophoresis using the Prep Cell apparatus (Bio-Rad). The purified sample was concentrated using a Millipore concentrator (Mw cutoff of 30,000). After filtration, the sample was used for the SAXS measurement. SAXS experiments were performed with NANOPIX (Rigaku).

RESULTS:

SAXS profiles of the *S. pombe* and human overlapping dinucleosomes are shown in Fig. 1. The *S. pombe* overlapping dinucleosome appeared to have a stretched structure, as compared to the human overlapping dinucleosome. A Guinier plot of the data for the *S. pombe* overlapping dinucleosome is shown in Fig. 2. The straight line represents the least-square fitting for the data. This result revealed that the gyration radius (R_g) of the *S. pombe* overlapping dinucleosome is 62.8 ± 1.2 Å, which is larger than that of the human canonical overlapping dinucleosome (R_g = 58.4 ± 1.2 Å).

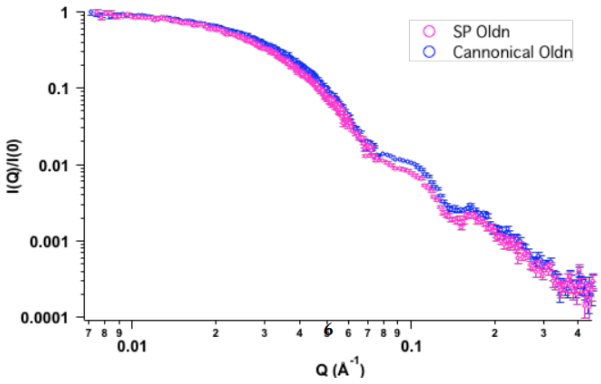

Fig. 1. SAXS profiles of the *S. pombe* (magenta) and human (blue) overlapping dinucleosomes.

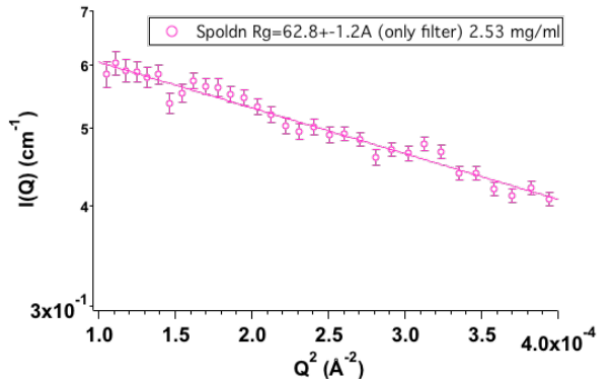

Fig. 2. A Guinier plot of the *S. pombe* overlapping dinucleosome.

REFERENCES:

[1] K. Luger *et al.*, Nature, **389** (1997) 251-260.
[2] M. Koyama and H. Kurumizaka, J. Biochem., **163** (2018) 85-95.
[3] D. Kato *et al.*, Science, **356** (2017) 205-208.
[4] M. Koyama *et al.*, Biochem. Biophys. Res. Commun., **482** (2017) 896-901.

CO6-3 Molecular Mechanism of the Interaction between Transcriptional Factors Sp1 and TAF4

E. Hibino, R. Inoue[1], M. Sugiyama[1], J. Kuwahara[2], K. Matsuzaki and M. Hoshino

Graduate School of Pharmaceutical Sciences, Kyoto University
[1]Research Reactor Institute, Kyoto University
[2]Faculty of Pharmaceutical Sciences, Doshisha Women's University

INTRODUCTION: The expression of genes is controlled in a temporally and spatially coordinated manner, and this precise regulation is accomplished by the interactions of a variety of transcriptional factors.

The promoter-specific transcription factor Sp1 plays a primary role in the regulation of more than 100 genes. Sp1 specifically recognizes the GC-rich consensus sequence, and binds to these promoter regions to increase the transcriptional levels of target genes. Sp1 contains two Q-domains in the middle of the molecule, and three zinc fingers at the C-terminus. Although the structures of Zn-finger motifs were revealed by high-resolution NMR spectroscopy, structural details on other regions including the two Q-domains have yet to be elucidated.

The fourth-element of the general transcriptional factors, TAF4, is involved in interactions with cellular transcriptional activators. Sequence analyses revealed that TAF4 possesses two highly conserved domains, CI and CII, as well as four Q-domains in the center of molecule. Whereas the X-ray structures are reported for CI and CII domains, only limited information is available on the structures of the four Q-domains although these Q-domains are involved in interactions with a number of gene-specific transcriptional activators, such as Sp1.

Here, we report the structural details of two Q-domains in Sp1 and four in TAF4, which are important for the interaction between these proteins.

EXPERIMENTS: The glutamine-rich fragment proteins of Sp1 (Sp1-QA, -QB, -QBn, -QBc), and TAF4 (TAF4-Q12, -CI, -Q34) were constructed as fusion protein with ubiquitin. The proteins were expressed and purified as described previously [1].

CD spectra were measured on a Jasco J-820 spectropolarimeter. An assembling cell composed of a pair of quartz plates with a 0.1-mm path length, was used to record spectra between 250 and 190 nm at a protein concentration of 50 μM at 25°C.

SAXS measurements were performed with the spectrometer installed at BL-10C of Photon Factory with a PILATUS 2M detector. The two-dimensional data were converted into a one-dimensional curve by a circulation average and the scattering profile, $I(q)$, of the protein was then obtained.

NMR experiments were performed on a Bruker Avance 600 spectrometer with triple-resonance probe. A typical ^{1}H-^{15}N HSQC experiments were performed at protein concentration of 50 mM. The solvent conditions used were 20 mM sodium acetate (pH 5.0), and 10% D2O. The chemical shift value was referenced to DSS.

RESULTS: We first measured the far-UV CD spectra of Q-domain fragment proteins of Sp1 and TAF4. All the spectra showed a large minimum at ~200 nm, suggesting that neither protein has rigid secondary structures. Next, we measured ^{1}H-^{15}N HSQC spectra for each fragment proteins. We found that the chemical shift dispersion was very poor and all the peaks were appeared within a narrow region between 7.6 and 8.6 ppm. We also analyzed the overall shape of the molecules by the small-angle X-ray scattering. The analysis of Guinier plots revealed that the proteins were largely expanded. Furthermore, the Kratky plots did not show any clear peak, suggesting that the molecules lack globular shape but are rather chain-like conformation. All these analyses (CD, NMR and SAXS) indicate that the Q-domains of Sp1 and TAF4 are categorized as the intrinsically disordered proteins (IDPs), which lack rigid secondary and tertiary structures under the physiological conditions.

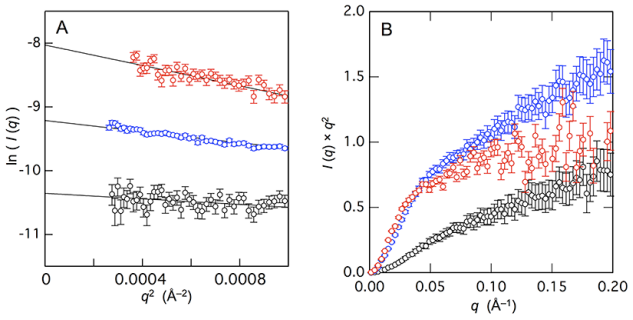

Fig. 1. The Guinier (A) and Kratky (B) plots of small-angle X-ray scattering of Sp1-QA (black), Sp1-QB (blue), and TAF4N/C (red) shown in open circles. The lines in (A) indicate the results of linear curve fitting for the data within the Guinier-region.

In order to examine whether the isolated Q-domains (Sp1-QA and QB) interact with the central part of TAF4 (TAF4N/C, containing all four Q-domains), the ^{1}H-^{15}N HSQC spectra were measured for ^{15}N-Sp1-QA and ^{15}N-Sp1-QB in the absence and presence of unlabeled TAF4N/C. In the case of ^{15}N-Sp1-QA, any change in the spectra was observed even in the presence of three-fold molar excess amount of unlabeled TAF4N/C. On the other hand, the intensity of several peaks in ^{15}N-Sp1-QB was significantly decreased by the addition of equimolar amount of TAF4N/C. We also analyzed the change in the chemical shift value upon the interaction in detail, and found that the binding site for TAF4N/C is located in the C-terminal region of Sp1-QB molecule. The results also suggested that the interaction between these proteins did not accompany with the significant conformational change in the molecules. This finding is not explained by the "coupled folding and biding mechanism", a widely accepted interaction mode for the IDPs and their ligands. The interaction between Sp1-QB and TAF4 might represent a novel binding mode for the IDPs.

REFERENCES:

[1] E. Hibino *et al.*, Protein Sci., **25** (2016) 2006-2017.
[2] E. Hibino *et al.*, Protein Sci., **26** (2017) 2280-2290.

CO6-4

Study of Localization Estimation of Abasic Sites in DNA Exposed to Radiomimetic Chemicals and ^{60}Co γ-rays

K. Akamatsu, N. Shikazono and T. Saito[1]

Radiation DNA Damage Research Group, Kansai Photon Science Institute, National Institutes for Quantum and Radiological Science and Technology (QST)

[1]Research Reactor Institute, Kyoto University

INTRODUCTION:

DNA lesions induced by ionizing radiation and chemicals can cause mutation and carcinogenesis. In particular, "clustered damage" site, that is a DNA region with multiple lesions within one or two helical turns, is believed to hardly be repaired. This damage is considered to be induced, *e.g.*, around high-LET ionizing radiation tracks. However, detail of the damage is not known. We have already developed a method for estimating degree of localization of abasic sites (APs) in DNA using Förster resonance energy transfer occurred between different fluorescence probes ("hetero-FRET" using Alexa350 and Alexa488) [1]. The results showed that $^{12}C^{5+}$ beam produced close APs within a track: the apparent distance calculated was approximately 17 base pairs [2]. This finding indicates that *direct radiation effect* of $^{12}C^{5+}$ beam near the Bragg peak produces clustered DNA damage. We have recently applied the method to DNA in a cell-mimetic radical scavenging condition. However, there are some problems of the complex protocol and of the sensitivity due to the low extinction coefficient of Alexa350. We have, therefore, developed "homo-FRET" occurred between two or more Alexa488 molecules. We will obtain magnitude of FRET also from "fluorescence anisotropy" of homo-FRET between Alexa488 molecules. The new protocol using homo-FRET [3] enables us to estimate DNA damage localization without any enzymes and improves sensitivity to detect a clustered damage.

EXPERIMENTS:

●*Sample preparation and irradiation*

The plasmid DNA digested by Sma I was used (linear form). The DNA was dissolved to be 0.1 g/L in 0.2 M Tris-HCl buffer (pH 7.5) which is a cell-mimetic condition in relation to radical scavenging capacity. Twenty microliters of the DNA solution was transferred to a microtube (0.5-mL size), and was irradiated with ^{60}Co γ-rays (LET: ~0.2 keV/μm; Kyoto University Research Reactor Institute: KURRI) as a standard radiation source. Moreover, the DNA solution was treated with so-called "radiomimetic" chemicals: MMS (methylmethanesulfonate, an alkylating agent) and NCS (neocarzinostatin, an antibiotic).

●*Preparation of fluorophore-labeled irradiated DNA and the FRET observation*

The damaged sample DNA (10 μL in water) and 10 μL of 100 mM Tris-HCl (pH 7.5) were mixed in a microtube. Two microliters of Alexa488/DMSO was added to the DNA solution and was incubated for 24 h at 35°C. The fluorophore-labeled DNA was purified by ethanol-precipitation followed by ultrafiltration. The fluorescence anisotropy was measured at 525 nm (ex. 470 nm).

The anisotropy, $< r >$, is defined as follows:

$$< r > = \frac{I_{VV} - G \bullet I_{VH}}{I_{VV} + 2G \bullet I_{VH}},$$

where I_{VV} is the fluorescence intensity when the excitation and emission polarizers are both vertically oriented. I_{VH} is one when the excitation/emission polarizers are vertically/horizontally oriented. G is the grating factor defined as I_{HV}/I_{HH}.

RESULTS AND DISCUSSION:

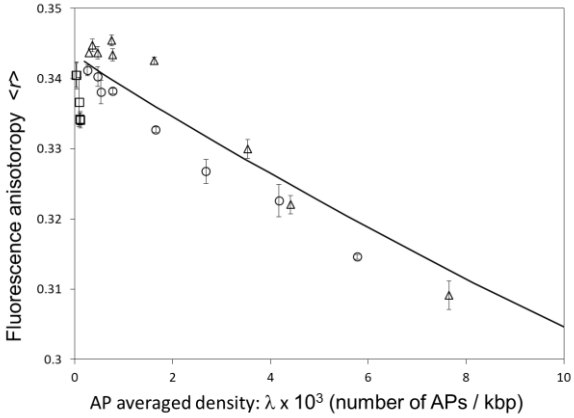

Fig. 1. Relationship between AP averaged density and fluorecence anisotropy for ^{60}Co γ-rays (○), MMS (Δ), and NCS (□). The solid line indicates a theoretical curve when APs are randomly distributed.

In general, fluorescence anisotropy decreases with increasing FRET [4]. As shown in Fig.1, we found that the relationship differed significantly among MMS, NCS, and ^{60}Co γ-rays. At lower AP density, MMS-inducing APs seemed to not be closely distributed, whereas NCS-induced APs were remarkably clustered. In contrast, the AP clustering by the γ-rays was similar to, but potentially more likely to occur than, random distribution. Here, we conclude that these radiomimetic chemicals are *not* radiomimetic at least in AP distribution. Now we apply the method to DNA irradiated with a variety of heavy ion beams such as He, C, and Fe, under cell-mimetic condition.

REFERENCES:

[1] K. Akamatsu, N. Shikazono, Anal. Biochem., **433** (2013) 171-180.
[2] K. Akamatsu, N. Shikazono, and T. Saito, Radiat. Res., **183** (2015) 105-113.
[3] K. Akamatsu, N. Shikazono, Anal. Biochem., **536** (2017) 78-89.
[4] L. W. Runnels, and S. F. Scarlata, Biophys. J., **69** (1995) 1569.

CO6-5 SAXS Study on the Structure of Prefibrillar Intermediates for the Formation of Insulin B Chain Amyloid Fibrils

N. Yamamoto, T. Akai, E. Chatani, R. Inoue[1], K. Morishima[1] and M. Sugiyama[1]

Graduate School of Science, Kobe University
[1]Research Reactor Institute, Kyoto University

INTRODUCTION: Amyloid fibrils are a form of protein aggregates with fibrous morphology and β-sheet-rich structure. Because of their deep association with a numerous number of diseases such as Alzheimer's disease and Creutzfeldt-Jacob disease, finding strategies for preventing aggregation is quite important from a perspective of the onset of above-mentioned diseases.

The formation of amyloid fibrils typically follows a nucleation-dependent polymerization, and a one-step nucleation has widely been accepted as the simplest scheme. On the other hand, various types of oligomers have been identified in the time domain of nucleation. This observation invokes the necessity of considering multi-step nucleation as another principle mechanism of amyloid nucleation, in which the formation of metastable prefibrillar intermediate species plays an important role [1].

We are attempting direct observation of such species, and recently, the formation of prefibrillar intermediates has been found in an insulin-derived peptide (insulin B chain) [2]. In this study, to elucidate structural properties of the prefibrillar intermediates, small-angle X-ray scattering (SAXS) measurements have been performed in combination with dynamic light scattering (DLS) experiments. Furthermore, we have analyzed changes in SAXS profiles after the addition of fibrinogen, a protein which has been revealed to function as the inhibitor of B-chain fibrillation [3].

EXPERIMENTS: Insulin B chain was dissolved in 50 mM Tris-HCl buffer at a concentration of 1.4 mg/ml, and was then put in a 1-mm path-length quartz cell. After 2-hour incubation at 25 °C to form the prefibrillar intermediate, the small angle X-ray scattering (SAXS) pattern was collected with NANOPIX (Rigaku Corporation, Japan) equipped with HyPix-6000. A Cu K-α line (MicroMAX-007HF) was used as a beam source, which was further focused and collimated with a confocal multilayer mirror (OptiSAXS). The camera length was set to 1.326 m and the range of the scattering vector q was from 0.0005 to 0.24 A^{-1}. In the structural analysis of the prefibrillar intermediate in the presence of fibrinogen, the prefibrillar intermediate formed by incubating 1.4 mg/ml insulin B chain for 2 hours was mixed with fibrinogen at a final concentration of 3.5 mg/ml and then subjected to the SAXS measurement.

RESULTS: Fig. 1 shows SAXS profiles of the prefibrillar intermediate of B chains and the complex of B chain and fibrinogen. The slope of the log-log plot of the scattering profile of the prefibrillar intermediate (circles) was close to −1, indicating that the prefibrillar intermediate has a rod-like structure. The analysis of cross-section plot suggested the approximate base radius of ~33 Å, and by using a diffusion coefficient determined by the DLS measurement, the length of the prefibrillar intermediate was estimated to be ~2,700 Å on the basis of Broersma's relationship, where a diffusion coefficient of a rod-like molecule is described by a function of the length and base radius. This result suggests that the peptide molecules of insulin B chain associated into rod-like prefibrillar intermediates in an early stage of the reaction. Preliminary time lapse monitoring of the amyloid formation reaction is now ongoing to investigate detailed time evolution of conformational development from monomers towards mature amyloid fibrils via the rod-like prefibrillar intermediate species.

As for the prefibrillar intermediate-fibrinogen complex, the slope of the log-log plot of the scattering profile (squares) was also close to −1, suggesting that the rod-like intermediate structure was kept even after the addition of the fibrinogen. The base radius and length of this complex form was calculated to be ~74 Å and ~2,900 Å, respectively. A slight increase of the base radius has provided a possible picture that a layer of fibrinogen is formed on the surface of the prefibrillar intermediates, shedding light on the inhibitory mechanism of fibrinogen on the B chain amyloid fibril formation.

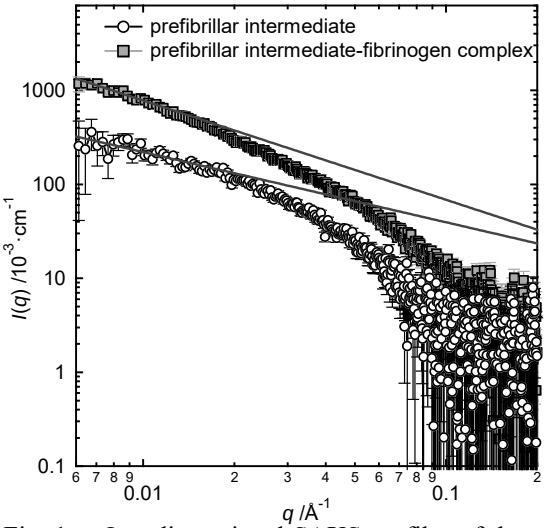

Fig. 1. One-dimensional SAXS profiles of the prefibrillar intermediate of insulin B chain (circles) and its complex with fibrinogen (squares).

REFERENCES:

[1] E. Chatani and N. Yamamoto, Biophys. Rev., **10** (2018) 527-534.
[2] N. Yamamoto *et al*., Sci. Rep., **8** (2018) 62.
[3] T. Akai, Master's Thesis, Kobe Univ. (2017).

CO6-6 Possible Involvement of Aspartyl L-to-D Isomerization of Cell Adhesion Molecule-1 Shedding Products in Neurodegeneration

A. Ito and N. Fujii[1]

Department of Pathology, Kindai University Faculty of Medicine

[1]Research Reactor Institute, Kyoto University

INTRODUCTION: Cell adhesion molecule 1 (CADM1) is a member of the immunoglobulin superfamily mediating intercellular adhesion. It is expressed in epithelial cells, such as lung alveolar and renal tubular cells, and widely in neurites of the central and peripheral nervus systems. CADM1 is enzymatically shed at the extracellular domain near the cell membrane. This phenomenon called ectodomain shedding is accelerated under some pathological conditions. In the lung of patients with pulmonary emphysema, a degenerative lung disease, CADM1 ectodomain shedding is increased in alveolar cells, and the resulting shedding products accumulate within the cells, then causing apoptosis [1,2]. This event appears to be involved in alveolar destruction, a hallmark feature of emphysema [1]. As CADM1 shedding occurs in nerves, it may be also involved in degeneration and/or apoptosis of neurons. Neuronal degeneration and apoptosis are common features of diseases caused by elevation of the intraluminal pressure, such as glaucoma and ventricular hydrocephalus.

EXPERIMENTS:
(1) A water pressure-loadable two-chamber culture system was originally devised by connecting a 60-cm-long plastic cylinder to the upper chamber in a water-proof manner [3,4]. This system can reproduce pathological conditions of the intraluminal pressure elevation. When cells are cultured in this system, they are to receive static medium-water pressure ranging up to 55 cmH_2O.
(2) Dorsal root ganglion neurons from C57BL/6 mouse neonates were cultured in the system, and were loaded with various degrees of water pressure for 1 to 3 days, when the neurons were sprouting many neurites to form elaborate neuritic networks.
(3) Protein was extracted from the resulting neuritic networks, and was subjected to Western blot analyses using an anti-CADM1 antibody.
(4) The resulting neuritic networks were also double stained with CADM1 immunofluorescence and mitochondrial labeling using the Mitotracker dye.

RESULTS:
(1) The intracellular product of CADM1 ectdoamin shedding (C-terminal fragment, CADM1-CTF) was increased in a manner dependent on the loaded water pressure.
(2) The more the loaded water pressure was, the less elaborate the neuritic networks were [Fig. 1]. In addition, the neurites became rough and course in their surface, and CADM1 immunostain signals were punctate [Fig. 1]. Some punctate CADM1 signals were colocalized with Mitotracker dye stains, which were also punctate or drop-like [Fig. 1].
(3) These results suggest that CADM1-CTF might preferentially aggregate with each other and might inhibit neuritic extension and cause neuritic degeneration.

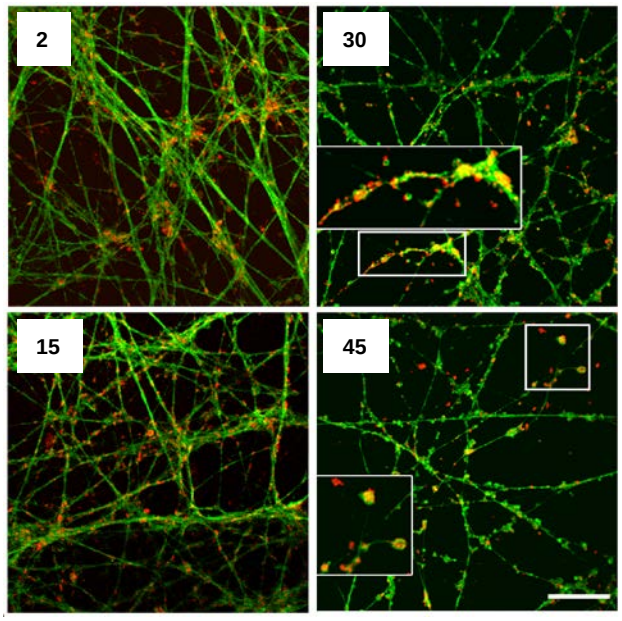

Fig. 1. Double staining of neuritic networks with CADM1 immunofluorescence (green) and mitochondrial labeling (red). Neuritic networks were developed for 3 days under the water pressure indicated (cmH_2O).

PERSPECTIVES:
CADM1-CTF contains an amino acid region very rich in aspartyl residues, *i.e.*, ADDAADAD. These aspartyl residues may be isomerized to D-form, because they are surrounded by alanine residues that have a small side chain. This D-isomerization may be a cause of molecular aggregation of CADM1-CTF in neurites, and thereby neuritic degeneration possibly through interfering with neuritic mitochondrial function. Future studies to prove this hypothesis will open a new avenue leading to better understanding of neurodegeneration caused by internal pressure elevation.

REFERENCES:
[1] T. Mimae *et al.*, Thorax, **69** (2014) 223-231.
[2] M. Hagiyama *et al.*, J. Biomed. Sci., **22** (2015) 67.
[3] A. Yoneshige *et al.*, Mol. Neurobiol., **54** (2017) 6378-6390.
[4] M. Hagiyama *et al.*, Front. Physiol., **8** (2017) 997.

CO6-7 Structural Characterization of Circadian Clock Potein Complexes

H. Yagi, Y. Yunoki, K. Morishima[1], N. Sato[1], R. Inoue[1], and M. Sugiyama[1]

Graduate School of Pharmaceutical Sciences, Nagoya City University,

[1]Institute for Integrated Radiation and Nuclear Science, Kyoto University

INTRODUCTION: The central oscillator that generates the circadian rhythm in the cyanobacterium comprises only three proteins—KaiA, KaiB, and KaiC. Through interactions among these proteins in the presence of ATP, KaiC undergoes phosphorylation and dephosphorylation cycles with the period of 24 h, which proceeds *in vitro* without daylight oscillation, indicating that the internal clock mechanism can be autonomous irrespective of transcriptional and translational feedback systems. Although the formation of several complexes, such as KaiA-KaiC, KaiB-KaiC, and KaiA-KaiB-KaiC oscillated in a circadian manner, their stoichiometry or the detailed structures remains to be elucidated. Herein, in order to understand the oscillation mechanism mediated by the clock protein complex, we characterized the complexes by using native mass spectrometry (nMS), nuclear magnetic resonance (NMR) spectroscopy and small angle scattering analysis.

EXPERIMENTS: The expression and purification of clock proteins, KaiA, KaiB and KaiC were performed according to methods previously described [1]. Small angle X-ray scattering (SAXS) pattern was collected with NANOPIX (Rigaku Corporation, Japan) equipped with HyPix-6000. A Cu K-α line (Mi-cro MAX-007HF) was used as a beam source, which was further focused and collimated with a confocal multilayer mirror (OptiSAXS) . The camera length was setto 1.326 m and the range of the scattering vector q was from 0.007 to 0.24 A-1. Deuteration-assisted small angle neutron scattering (SANS) experiments were performed using the D22 instrument installed at the Institut Laue-Langevin (ILL), Grenoble, France.

RESULTS:

KaiB-KaiC complex

The nMS titration data showed that the proteins formed a complex exclusively in a 6:6 stoichiometry, indicating that KaiB bound to the KaiC hexamer with strong positive cooperativity. The inverse contrast-matching SANS measurement indicated that the disk-shaped arrangement of the KaiB subunits on the outer surface of the KaiC ring, which also serves as the interaction site for SasA, a histidine kinase that operates as a clock-output protein in the regulation of circadian transcription. These data suggest that cooperatively binding KaiB competes with SasA with respect to interaction with KaiC, thereby promoting the synergistic release of this clock-output protein from the circadian oscillator complex.

KaiA-KaiC complex

KaiC binds 12 ATP to form a hexamer and possesses ATPase related to autokinase and autophosphatase activities. Herein, we characterized changes in structure and the KaiA-binding affinity of KaiC depending on its nucleotide state resulting from ATP hydrolysis. In this study, we controlled the nucleotide state using non-hydrolysable ATP analog (AMPPNP). The nMS analyses indicated that a KaiC hexamer formed with AMPPNP exhibits a lower affinity to KaiA in comparison with that formed with ATP. The data indicated that ATP hydrolysis in the KaiC hexamer promotes its interaction with KaiA presumably through KaiC's conformational change in KaiA binding region. In the SAXS experiment, the overall structural change was not observed upon ATP hydrolysis (Fig. 1). It has been reported that KaiA interacts with flexible C-terminal region on KaiC. Indeed, our NMR data indicated that the C-terminal region underwent structural change depending on ATP hydrolysis, and moreover was involved in interaction with KaiA.

On the basis of these data, we conclude that ATP hydrolysis in the KaiC hexamer causes its conformational changes in the KaiA-binding site, endowing it with high-affinity for KaiA. These findings provide mechanistic insights into the circadian periodicity in cyanobacteria.

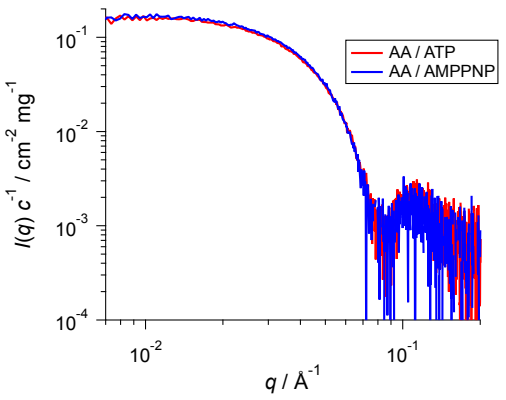

Fig. 1.The SAXS profiles of dephosphorylated mutant KaiC hexamers fomed with ATP (red) and AMPPNP (blue).

REFERENCE:[1] M. Sugiyama *et al.*, Sci. Rep., Article number: 35567 (2016).

CO6-8 Measurement of Trancemitance Spectra of a Humann Calcificated Aorta Tissue in the Sub-Terahertz Region

N. Miyoshi and T. Takahashi[1]

Department of Molecular Chemistry, Kyoto Institute of Technology
[1]Institute for Integrated Radiation and Nuclear Science, Kyoto University

INTRODUCTION: The LINAC (Electron linear accelerator) technology in the millimeter- and terahertz-waves had been unique and had been used as a coherent synchrotron light source in the Institute for Integrated Radiation and Nuclear Science of Kyoto university (KURNS) to observe the transmittance spectra of a human calcified aorta tissue as a collaborate study. The absorption spectra in the sub-terahertz region had been not so clear for the raw tumor tissue although Ashworth-PC. *et al.* [1] had reported for the excised human breast cancer by a terahertz pulsed spectroscopy observed at 320 GHz, which was estimated a longer relaxation time component of the induced electricity for water molecules [2-3] in the raw tumor tissue for three years at the linear analysis.

We estimated what kind of water molecules become dominant in the viable and necrotic cancer regions by the different measurement method as an aim of 2D mapping study comparing with the pathological staining H&E imaging. In the results, it is considered that the molecule of the water presented in the necrotic area will be different one of the normal tissue, which looks to be near closed one of free water in the necrotic area at 600 GHz (the fast relaxation time) which was reported by Dr. H. Yada [3] beside of 4-5 THz. The other components at 200-400 GHz were also presented in the raw tumor tissues as un-known components [2], which was very interesting ones about the water molecules in the necrotic environment.

EXPERIMENTS: (1) Instrument of Near-field in Terahertz Region: The photograph of the instrument was shown in Fig. 1. Mark-A: Pre-probe Wiston cone; 50-10mm diameter, Length=60mm; the irradiate diameter=0.775mm; Mark-B: The concentrate light probe (diameter=3mm). The instrument was developed by Dr. T. Takahashi [4] for the transmittance measurements.

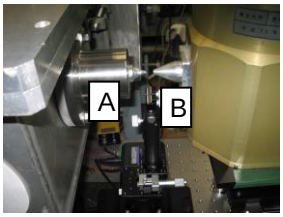

Fig. 1. The near field area of sample holder position.

(2) Sample Preparation: A calcified aorta blood vessel wall tissues were supplied by pathological autopsy. The sample tissues were dried with air in the room temperature as Fig. 2.

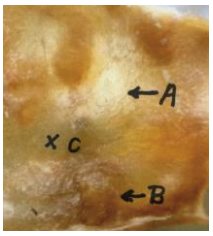

Fig. 2. The sample photograph of a human calcified aorta blood vessel wall tissue suplied from an autopsy. (A: calcified; B: choresterol; C: normal blood vessel wall tissues)

RESULTS:
The transmittance spectra of the sample tissue for each points A, B and C were measured as shown in Fig. 3.

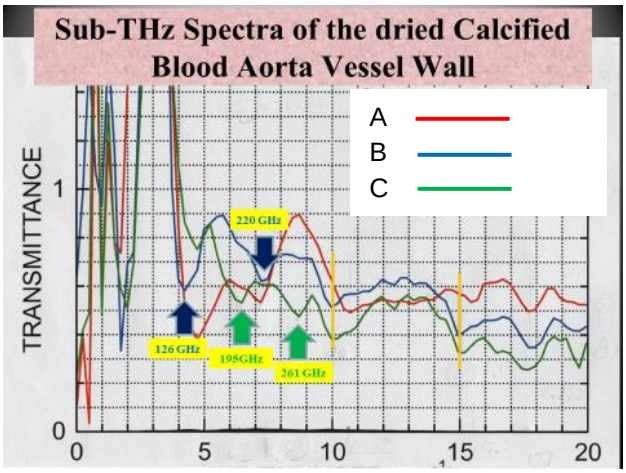

Fig. 3. Sub-THz spectra of the dried calcified blood aorta vessel wall.
(A: calcified; B: cholesterol; C: normal)

In the results, the absorbance of the dried tissue at 195 and 261 GHz were observed in the calcified area (included of PO_4 components), and the absorption peaks of 125, 220 GHz were observed in the cholesterol (included of C-H and C-H_2 components) adhesion area.

In the both areas, it was observed the absorption peaks at 300 and 450 GHz also.

In future, it will be needed more measurements and analysis of these spectra.

REFERENCES:

[1] Phillip C. Ashuworth *et al.*, Optics Express, **17** (2009) 12444-12454.
[2] Toshiko Fukasawa, *et al.*, Phys. Rev. Lett., **95** (2005) 197802.
[3] Hiroyuki Yada, *et al.*, Chem. Phys. Lett., **464** (2007) 166-170.
[4] T. Takahashi, *et al.*, J. Phys.: Conf. Ser. **359** (2012) 012016-1-4.

CO6-9 Study of the Radioresistance Mechanisms of Radioresistant Bacteria

T. Saito

Institute for Integrated Radiation and Nuclear Science, Kyoto University

INTRODUCTION: There are various environments in nature, and organisms have evolved diversely to be able to adapt to most of these environments. Some organisms can survive in environments that are considered extremely severe by our common sense. Elucidation of the adaptive mechanisms of organisms to severe environments can provide meaningful information about the evolution and diversity of whole organisms. Some bacteria, known as radioresistant bacteria, have extremely high resistance to ionizing radiation [1]. Their resistance to such extreme conditions makes radioresistant bacteria an interesting area in research. In order to elucidate the mechanisms underlying this radioresistance, it is important to study the organisms' defense mechanisms at a molecular level against external stress. However, the study of these organisms in nature can be very challenging, as the knowledge on their genetic and biochemical properties is still inadequate. In this study, generation of radioresistant *Escherichia coli* cells by an experiment on the adaptive evolution to gamma rays was attempted. In this experiment, the following steps were performed: gamma-ray irradiation of *E. coli* cells whose genetic and biochemical properties are well known, growth of surviving cells, and irradiation of the grown cells.

EXPERIMENTS: Evaluation of the sensitivity of *E. coli* cells to gamma rays: *E. coli K*-12 cells were grown to the early log phase in LB medium at 37°C at 200 rpm. One milliliter of culture was centrifuged at 4000 × *g* at 20°C for 10 min. The supernatant was discarded and the pellet was suspended in 1 mL of PBS(–). The cell suspension was irradiated with gamma rays at a dose rate of 21 Gy/min at room temperature. Gamma irradiation was carried out at the Co-60 Gamma-ray Irradiation Facility of the Institute for Integrated Radiation and Nuclear Science, Kyoto University. The gamma-irradiated cell suspension was diluted appropriately with PBS(–), plated on LB agar, and incubated at 37°C for 12 hr. Colonies were counted, colony forming units were determined, and survival rates were calculated.

Selection with gamma rays: A single colony of *E. coli K*-12 clone cells was suspended in LB medium and grown to the early log phase at 37°C at 200 rpm. The cell suspension was prepared as described above. The cell suspension was irradiated with the 1% survival dose of gamma rays at a dose rate of 21 Gy/min at room temperature. One milliliter of gamma-irradiated cell suspension was inoculated in 100 mL LB medium and grown to the early stationary phase at 37°C at 200 rpm. Glycerol stock was prepared and stored at –80°C. This protocol was repeated with cells from the glycerol stock grown to the early log phase.

RESULTS: In order to generate *E. coli* cells radioresistant to gamma rays by adaptive evolution, which were used as the selection pressure, *E. coli* cells were irradiated with a 1% survival dose of gamma rays, and the surviving cells were grown. The 1% survival dose of the surviving cell population to the same radiation was evaluated, and the cell population was once again irradiated with the 1% survival dose. An increasing trend in radioresistance of the *E. coli* cell population was observed when the experiment was repeated six times. The *E. coli* cell population with 3.4-fold resistance to gamma rays compared to the cells without selection was obtained by repeating the experiment eight times (Fig. 1). However, no further increase in radioresistance was observed in the *E. coli* cell population when the experiment was repeated ten times (Fig. 1). These results indicate that an evolutionary plateau exists in the process of adaptive evolution of *E. coli,* when gamma rays are used as selection pressure. Further studies should be conducted to generate *E. coli* cells resistant to higher doses of gamma rays by additional repetitions of the selection cycle and to analyze the genetic and biochemical properties of the resulting *E. coli* cells. These experiments will be required to further understand the biological defense mechanisms of radioresistant bacteria to ionizing radiation.

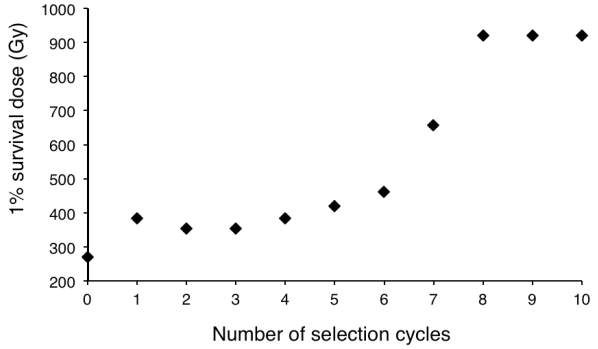

Fig. 1. One percent survival doses of *E coli* cell populations to gamma rays evaluated at each selection cycle.

REFERENCE:

[1] T. Saito, Viva Origino, **30** (2007) 85–92.

CO6-10 Conformational Characterization of Archaeral Homolog of Proteasome-assembly Chaperone PbaA

M. Yagi-Utsumi, R. Inoue[1], N. Sato[1], M. Sugiyama[1] and K. Kato

Institute for Molecular Science, National Institutes of Natural Sciences
[1]Institute for Integrated Radiation and Nuclear Science, Kyoto University

INTRODUCTION: Recent bioinformatic analyses identified proteasome assembly chaperone-like proteins, PbaA and PbaB, in archaea. PbaB forms a homotetramer and functions as a proteasome activator, whereas PbaA does not interact with the proteasome despite the presence of an apparent C-terminal proteasome activation motif [1, 2]. The C-terminal α6 helices of the PbaB tetramer show tentacle-like structures that project from the core domain, whereas the corresponding C-terminal helical segments of a PbaA pentamer are packed against the core. These structural features may explain the distinct proteasome-binding capabilities of PbaA and PbaB, although the conformational difference may be due to different modes of crystal packing.

In this study, we characterized the quaternary structure of PbaA in solution by small-angle X-ray scattering (SAXS) and high-speed atomic force microscopy (HS-AFM). Moreover, we attempted to endow PbaA with proteasome-binding activity by mutational modifications of its C-terminal segment based on our structural data and examined the structural impact of the mutations using biophysical techniques.

EXPERIMENTS: The expression and purification of *P. furiosus* PbaA, PbaB and the 20 S proteasome were performed according to methods previously described [1, 2]. Three constructs encoding PbaA–PbaB chimeric proteins were created by replacing the C-terminal segment of PbaA with that of PbaB. SAXS experiments were performed with NANOPIX (Rigaku) at 20°C. X-rays from a high-brilliance point-focused X-ray source (MicroMAX-007HF) were focused and collimated with a confocal multilayer mirror (OptiSAXS) and low parasitic scattering pinhole slits (ClearPinhole). The scattered X-rays were detected using a two-dimensional semiconductor detector (HyPix-6000). The SAXS pattern was converted to a one-dimensional scattering profile, and then standard corrections were applied for initial beam intensity, background scattering and buffer scattering. X-ray crystal structure analyses of PbaA, HS-AFM, and the proteasome activation assay were also performed.

RESULTS: We revealed that PbaA forms a homopentamer predominantly in the closed conformation with its C-terminal segments packed against the core domains (Fig. 1), in contrast to the PbaB homotetramer with projecting C-terminal segments. This prompted us to create a novel proteasome activator based on a well-characterized structural framework. We constructed a panel of chimeric proteins comprising the homopentameric scaffold of PbaA and C-terminal segment of PbaB and subjected them to proteasome-activating assays as well as SAXS and HS-AFM. The results indicated that the open conformation and consequent proteasome activation activity could be enhanced by replacement of the crystallographically disordered C-terminal segment of PbaA with the corresponding disordered segment of PbaB [3]. Moreover, these effects can be produced just by incorporating two glutamate residues into the disordered C-terminal segment of PbaA, probably due to electrostatic repulsion among the negatively charged segments. Thus, we successfully endowed a functionally undefined protein with proteasome-activating activity by modifying its C-terminal segment.

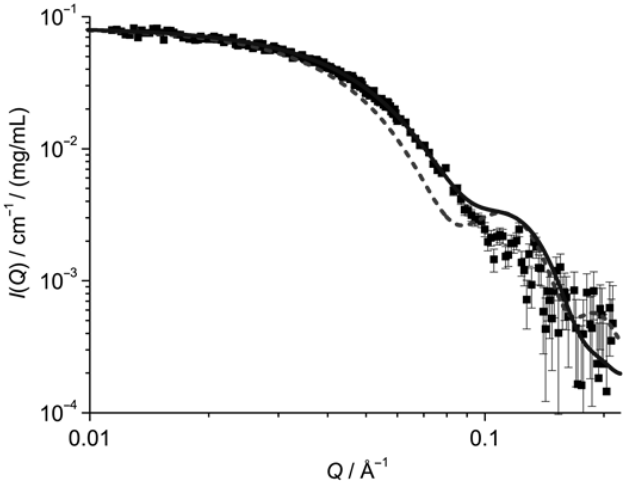

Fig. 1. The SAXS profile calculated from the crystal structures of the closed conformation of PbaA (solid line) and the open conformation of PbaA (dashed line), along with the experimentally obtained profile (black square).

REFERENCES:

[1] K. Kumoi *et al.*, PLoS ONE, **8** (2013) e60294.
[2] A. Sikdar *et al.*, Biochem. Biophys. Res. Commun., **453** (2014) 493-497.
[3] M. Yagi-Utsumi *et al.*, Protein Eng. Des. Sel., **31** (2018) 29-36.

CO6-11 Dynanic Light Scattering of Ribonuclease A

S. Fujiwara, K. Morishima[1], T. Matsuo, F. Kono, T. Chatake[1], R. Inoue[1] and M. Sugiyama[1]

Quantum Beam Research Science Directorate, National Institutes for Quantum and Radiological Science and Technology

[1]Research Reactor Institute, Kyoto University

INTRODUCTION: Proteins are constantly fluctuating under the influence of thermal fluctuations of surrounding solvent molecules. These fluctuations, or the dynamics, of the proteins are known to indispensable to the structural changes that enable the proteins to function [1]. Full understanding of the molecular mechanisms of the functions of the proteins thus requires understanding of the dynamics as well as the structures of the proteins.

The dynamics of the proteins spans from the fluctuations of the polypeptide side chains through motions of the disordered segments in the polypeptide chains and the domain motions to diffusion of the entire protein [2]. Elucidating how the dynamics at these different levels are related to each other is important to elucidate the relationship between the dynamics and the structures.

Quasielastic neutron scattering (QENS) provides a tool to directly measure the dynamics of the proteins. We have noticed that QENS contains information on the segmental motions and the domain motions as well as the diffusion of the entire molecules and the local motions of the side chains [3,4]. Although the local motions can be separated, attempts to separate the segmental and domain motions from the diffusion of the entire molecules have not been made because both contribute to the broadening of the elastic peak. To separate the contribution of the segmental and domain motions, the information on the diffusion of the entire molecules is required. Dynamic light scattering (DLS) provides this information. From the DLS measurements of the protein solutions, the translational diffusion coefficients can be estimated. Since the DLS measurements can be carried out under the condition similar to the QENS measurements, DLS and QENS are well suited as the complementary measurements.

EXPERIMENTS: As part of the project measuring the dynamics at the different structural levels of the proteins, we carried out the DLS measurements of protein solutions. We employed ribonuclease (RNase) A as a typical globular protein (the folded state). We also prepared the molten-globule (MG) and unfolded states of RNase A as samples with different degrees of the segmental motions. The measurements were carried out using a system consisting of a 22 mW He-Ne laser (wavelength 632.8 nm), an avalanche photodiode mounted on a static/dynamic compact goniometer, ALV/LSE-5003 electronics and an ALV-5000 correlator.

RESULTS: Figure 1 shows an example of the decay time distributions of the folded, MG, and unfolded states of RNase A, obtained by the CONTIN analysis [5]. The distributions with a single peak indicate that the solution in each state is monodisperse.

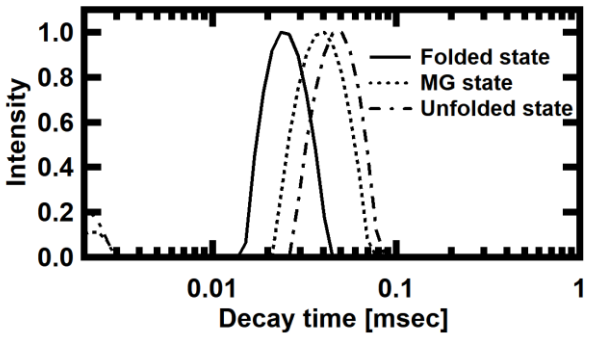

Figure 1. Example of the decay time distributions of RNase A. The distributions at the scattering angle of 90 degrees are shown.

Figure 2 shows the Q (= $(4\pi n_0/\lambda)\sin\theta$, where n_0 is the refractive index, λ is the wavelength, and 2θ is the scattering angle) dependences of the decay rates (the inverse of the decay time). These curves are well fit with straight lines, from the slopes of which the translational diffusion coefficients can be estimated.

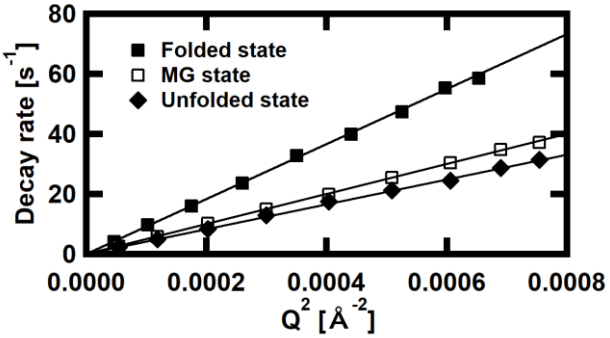

Figure 2. The Q-dependences of the decay rates. The liner fits to the curves are shown.

The translational diffusion coefficients of the folded, MG, and unfolded states were found to be 9.1×10^{-7} cm^2/s, 5.0×10^{-7} cm^2/s, and 4.2×10^{-7} cm^2/s, respectively. These values provide the important information on the extraction of the contribution of the segmental and domain motions in the QENS spectra.

REFERENCES:

[1] G. Zaccai, Science, **288** (2000) 1604-1607.
[2] K. Henzler-Wildman *et al*., Nature, **450** (2007) 964-972.
[3] S. Fujiwara *et al.*, PLOS ONE, **11** (2016) e0151447.
[4] S. Fujiwara *et al.*, J. Phys. Chem. B, **121** (2017) 8069-8077.
[5] S.W.A. Provencher, Comp. Phys. Comm., **27** (1982) 213-227.

CO6-12 Characterization of Conformational Deformation-coupled Interaction between Immunoglobulin G1 Fc Glycoprotein and a Low-affinity Fcγ Receptor

S. Yanaka, R. Yogo[1], R. Inoue[2], N. Sato[2], M. Sugiyama[2], and K. Kato

Institute for Molecular Science, National Institutes of Natural Sciences
[1]Graduate School of Pharmaceutical Sciences, Nagoya City University
[2] Institute for Integrated Radiation and Nuclear Science, Kyoto University

INTRODUCTION: A recently developed integrative approach combining varied types of experimental data has been successfully applied to three-dimensional modelling of larger biomacromolecular complexes. Deuteration-assisted small-angle neutron scattering (SANS) plays a unique role in this approach by making it possible to observe selected components in the complex. It enables integrative modelling of biomolecular complexes based on building-block structures typically provided by X-ray crystallography. In this integrative approach, it is important to be aware of the flexible properties of the individual building blocks.

EXPERIMENTS: Here we examine the ability of SANS to detect a subtle conformational change of a multidomain protein using the Fc portion of human immunoglobulin G (IgG) interacting with a soluble form of the low-affinity Fcγ receptor IIIb (sFcγRIIIb) as a model system. The IgG-Fc glycoprotein was subjected to SANS in the absence and presence of 75%-deuterated sFcγRIIIb, which was matched out in D_2O solution.

RESULTS: Inverse contrast-matching technique enabled selective observation of SANS from IgG-Fc, thereby detecting its subtle structural deformation induced by the receptor binding (Fig.1). The SANS data were successfully interpreted by considering previously reported crystallographic data and an equilibrium between free and sFcγRIIIb-bound forms. Our SANS data thus demonstrate the applicability of SANS in the integrative approach dealing with biomacromolecular complexes composed of weakly associated building blocks with conformational plasticity.

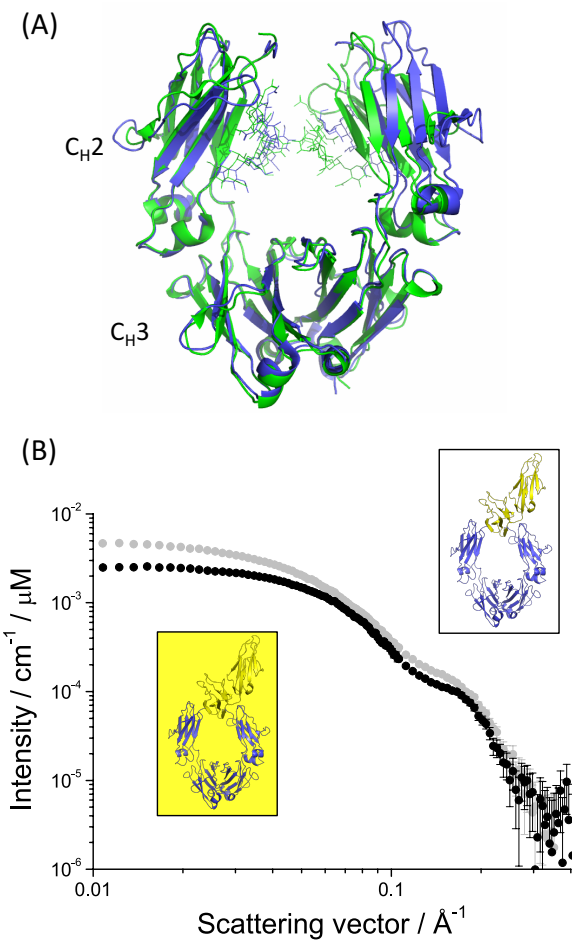

Fig. 1. structural deformation of IgG-Fc induced by the receptor binding

(A) Superposition of crystal structures of Fc in free (PDB code 3AVE) and sFcγRIIIb-bound states (PDB code 1T89).
(B) SANS profiles for Fc in in the presence of non-deuterated sFcγRIIIb (gray circles) and Fc in the presence of 75%-deuterated sFcγRIIIb (black circles) in 99.8% D_2O. Graphical models illustrate deuteration (colored gray) of solvent and protein based on the crystal structure of the Fc-sFcγRIIIb complex (PDB code 1T89)

REFERENCE:

[1] R. Yogo *et al.*, Biochem. Biophys. Rep. **12** (2017) 1-4.

CO6-13 ATP-dependent Solution Structure of Multi-domain Protein, MurD

H. Nakagawa, T. Saio[1,2], M. Sugiyama[3] and R. Inoue[3]

Materials Science Research Center, Japan Atomic Energy Agency

[1]*Graduate School of Chemical Sciences and Engineering, Hokkaido University*

[2]*Department of Chemistry, Faculty of Science, Hokkaido University*

[3]*Research Reactor Institute, Kyoto University*

INTRODUCTION: In structural biology, precise de-termination of three-dimensional structures of proteins has been focused, and the structures with an atom-ic-resolution have given solid platforms to understand their biological functions. Recently, the idea of structural biology has extended beyond the static structural infor-mation with atomic resolution, in order to cover more complex and dynamical structures at different levels of space and time resolution. SAXS measurement can ob-serve the solution structure of flexible protein under the physiological conditions [1].

MurD (UDP-N-acetylmuramoylalanine--D-glutamate ligase) is a typical multi-domain protein (Fig.1), which is one of the ATP-driven Mur ligases that are responsible for peptidoglycan biosynthesis. The crysital structure of MurD has been determined, but the ATP-bound form is not detemied.

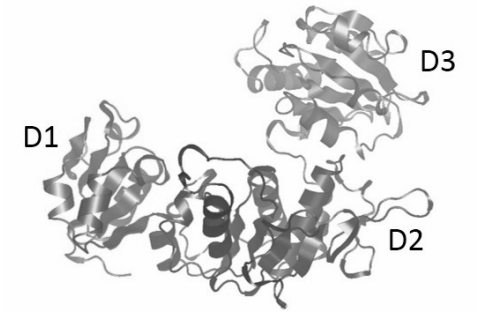

Fig. 1. Multi-domain protein, MurD, which are composed of three domains, D1, D2 and D3.

EXPERIMENTS: MurD were expressed in E. coli strain BL21 (DE3). Small angle X-ray scattering (SAXS) were measured for MurD in ATP-unbound and bound states at the concentration of 5, 10, 20 and 50 mg/ml. The buffer conditions were 20 mM Tris-HCl at pH=7.2. For the sample of ATP-bound states, AMP-PNP and $MgCl_2$ were added at the concentration of 2 mM and 5 mM, re-spectively.

RESULTS: SAXS profiles of MurD were successfully obtained for ATP-bound and unbound states. At the high-er concentrations, the inter-particle interaction effects were observed in the profiles. And it was found that un-der 10 mg/ml, the effect can be negligible. As shown in Fig. 2, SAXS profiles are different between ATP-bound and unbound states, indicating the structural change by ATP binding. The previous NMR measurement predicted that the domain orientation of MurD is changed by ATP binding [2]. And our preliminary MD simulation shows the ATP-dependent structural and motional change of MurD domain, and these results should be consistent with the NMR results. The comparison of the SAXS profiles with the results of the NMR and MD simulation are in progress.

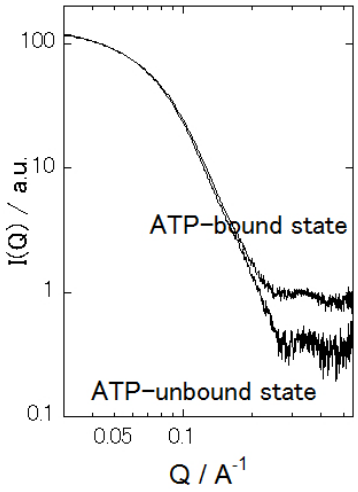

Fig. 2. SAXS profiles in ATP-bound and unbound states of MurD at the concentration of 10 mg/ml.

REFERENCES:

[1] J. Trewhella *et al.*, Acta Cryst. **D73** (2017) 710-728.
[2] T. Saio *et al.*, Sci. Rep., **5** (2015) 16685.

CO6-14 Production of Medical Radioisotopes Using Electron Linear Accelerator

S. Sekimoto, T. Ohtsuki

Research Reactor Institute, Kyoto University

INTRODUCTION: A shortage in the supply of ^{99}Mo resulting from the shutdown of reactors used for its production is a global problem. Because ^{99}Mo is an indispensable source of ^{99m}Tc, which is used in nuclear medicine to make diagnoses using techniques such as scintigraphy and single photon emission computed tomography (SPECT), a stable supply of ^{99}Mo is vital. Therefore, production of ^{99}Mo by using neutrons or protons generated in accelerators has been investigated [1–3]. To separate ^{99m}Tc from ^{99}Mo produced by an accelerator, methods based on sublimation, solvent extraction, and ion-exchange column chromatography have been examined and developed [2,4–6]. In addition, Gopalakrishna et al. have reported the preparation of ^{99}Mo by the ^{100}Mo(γ,n) reaction using bremsstrahlung photons [6], followed by conventional solvent extraction using methyl ethyl ketone (MEK) and zirconium (Zr) molybdate gel to separate ^{99m}Tc. According to the regulations of the Japanese pharmacopeia, the extraction using organic materials and the gel method using heavy metal elements such as Zr are not approved for the ^{99m}Tc-separation methods. Additionally, it is also difficult and impractical to use the sublimation method, which requires complicated and/or large scale devices for the mass-production of pure ^{99m}Tc.

In this work, we carried out the production of ^{99}Mo by the ^{100}Mo(γ,n) reaction using bremsstrahlung photons generated in an electron linear accelerator (LINAC), a technique that has not been investigated significantly in Japan. The amounts of ^{99}Mo produced at several electron energies (E_e) were examined.

EXPERIMENTS: Powdered molybdenum oxide of about 20 mg ($^{100}MoO_3$, 99.01% isotopic enrichment, ISOFLEX, USA) was sealed in a high-purity aluminum foil and shaped into a pellet of 10 mm diameter. Each pellet stacked between the gold foils was enclosed in a quartz tube. The gold foils (10 mm ϕ × 0.02 mm thickness) were used as a fluence monitor for bremsstrahlung photons. The stacked samples in the quartz tube were irradiated by bremsstrahlung photons generated by a platinum converter (2 mm thickness) and cooled with running tap water. The irradiation was carried out using the LINAC at the Kyoto University Research Reactor Institute (KURRI). For five $^{100}MoO_3$ pellets, the accelerator was operated for 5 min with electron energies (E_e) of 21, 25.5, 32, 35, and 41 MeV and mean currents of 60, 44, 90, 34, and 36 μA, respectively. After the irradiation, the five $^{100}MoO_3$ pellets were weighed and resealed in new (non-irradiated) aluminum foil pieces that were shaped into pellets of 10 mm diameter for γ-ray counting.

The γ rays of ^{99}Mo (740 keV) produced by the ^{100}Mo(γ,n) reaction in the irradiated $^{100}MoO_3$ pellet were measured using a Ge detector at KURRI. Measurements of 400–20,000 s were repeated several times within a week. The irradiated $^{100}MoO_3$ pellets were placed at the appropriate distance from the Ge detector surface to maintain a dead time of <10%. The activity of the ^{99}Mo produced in each irradiated $^{100}MoO_3$ pellet was estimated from the counting efficiency that was obtained from the radioactivity of the mixed standard sources.

RESULTS: The measured activities of ^{99}Mo produced by the ^{100}Mo(γ,n) reaction using bremsstrahlung photons, which were generated at E_e's of 21, 25.5, 32, 35, and 41 MeV at the LINAC, are shown in Fig. 1. The irradiation time, beam current of electrons, and amount of target material ($^{100}MoO_3$) were normalized to 5 min, 100 μA, and 10 mg, respectively. Generally, the activity of ^{99}Mo increases as the E_e increases. The amount of ^{99}Mo produced by the ^{100}Mo(γ,n) reaction has not previously been reported, an exception being the values for E_e of 25 and 35 MeV reported by Sabelnikov et al. [7] and Mang'era et al. [5], respectively. These values can be compared with those obtained by us. By comparing these values, we found an inconsistency between our values and those of the literature that have been normalized to the same irradiation time, beam current of electrons, and amount of target material used in our experiments. The literature values were higher than ours at E_e's of 25 and 35 MeV by a factor of 2–3. This inconsistency can be explained by the differences in the experimental systems, *e.g.*, converters generating photons, intensity, and/or dispersion of photon beams.

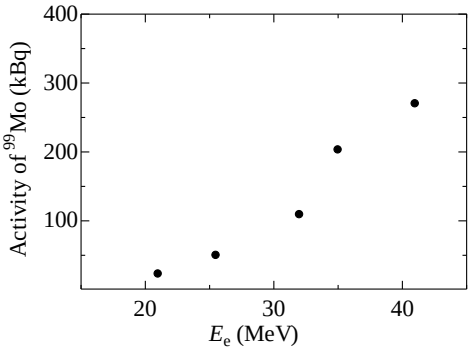

Fig. 1. Activity of ^{99}Mo produced using electron linear accelerator

REFERENCES:

[1] Y. Nagai *et al.*, J. Phys. Soc. Jpn. , **82** (2013) 064201.

[2] Y. Nagai *et al.*, J. Phys. Soc. Jpn. , **83** (2014) 083201.

[3] K. Nakai *et al.*, Proc. Jpn. Acad. Ser. **B 90** (2014) 413–421.

[4] M. Kawabata *et al.*, J. Phys. Soc. Jpn. , **84** (2015) 023201.

[5] K. Mang'era *et al.*, J. Radioanal. Nucl. Chem., **305** (2015) 79-85.

[6] A. Gopalakrishna *et al.*, J. Radioanal. Nucl. Chem., **308** (2016) 431-438.

[7] A.V. Sabel'nikov *et al.*, Radiochemistry, **48** (2006) 19–194.

29078

CO6-15 Chatacterization of Resonance Hybrid of Fe-bound Oxygen in Myoglobin

K. Hasegawa, M. Saito[1], M. Seto[1], Y. Kobayashi[1], T. Ohta[2], S. Yanagisawa[2], T. Ogura[2], Y. Yamamoto, T. Shibata, S. Neya[3] and A. Suzuki[4]

Department of Chemistry, University of Tsukuba

[1] Research Reactor Institute, Kyoto University
[2] Graduate School of Life Science, University of Hyogo
[3] Graduate School of Pharmaceutical Sciences, Chiba University

[4] Department of Materials Engineering, Nagaoka National College of Technology

INTRODUCTION: Oxygen (O_2) affinity of myoglobin (Mb) is regulated through heme electronic structure as well as heme environment furnished by nearby amino acid residues. We found that the intrinsic reactivity of heme Fe atom in the protein is affected by the electron density of the heme Fe atom (ρ_{Fe}) in a manner that the O_2 affinity decreases with decreasing the ρ_{Fe}.[1] This finding could be interpreted in terms of the effect of a change in the ρ_{Fe} on the resonance between Form A ↔ Form B of oxyMb (Scheme 1A). In this study, we measured Mössbauer spectra of oxyMbs reconstituted with Proto, Meso, 3,8-DMD, 7-PF, and 2,8-DPF (oxyMb(Proto), oxyMb(Meso), oxyMb(3,8-DMD), oxyMb(7-PF), and oxyMb(2,8-DPF), respectively) (Figure 1). These heme cofactors differ in the numbers of CF_3, CH_3, and C_2H_5 side chains, and the substitution of strongly electron - withdrawing trifluoromethyl (CF_3) group(s), as side chain(s) of heme cofactors, causes large and stepwise alterations of the heme electronic structure. The formal charges of heme Fe atom in Forms A and B are +2 and +3, respectively(Scheme 1A), and hence the effect of changes in the ρ_{Fe}, due to the chemical modifications of the heme cofactors, on the resonance between Form A ↔ Form B could be analyzed through the resonance hybrid of the formal charge of heme Fe atom reflected in the quadrupole splitting (QS) determined by the Mössbauer spectra.

EXPERIMENTS: Iron-^{57}Fe (95 atom %, Merck) was used to prepare ^{57}Fe-enriched heme cofactors. ApoMb was prepared from sperm whale Mb, using the standard procedure, and reconstituted with ^{57}Fe-labelled heme cofactors. 2 mM oxyMbs in 50 mM potassium phosphate buffer, pH 7.40, were cooled in liquid nitrogen bath. The Mössbauer measurements were performed at 3-6 K.

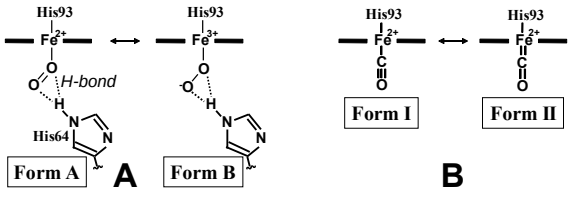

Scheme 1. Resonance between the two canonical forms A and B of the Fe-O_2 fragment in oxyMb (A) and that between forms I and II of the Fe-CO fragment in carbon moxide (CO) adduct of the protein (B). In (A), the formal charges of heme Fe atom in Forms A and B are +2 and +3, respectively. In (B), the resonance is affected by the electron density of the heme Fe atom (ρ_{Fe}).

RESULTS: The Mössbauer spectra of oxyMbs reconstituted with ^{57}Fe-labeled native and some chemically-modified heme cofactors (Figures 1) indicated that the heme cofactors are ranked as 2,8-DPF < 7-PF ≈ Proto < 3,8-DMD < Meso, in order of increasing QS, although their isomer shifts were similar to each other. The determined QS values correlated well with the stretching frequencies of Fe-bound CO (ν_{CO}) of carbon monoxide (CO) adducts of the proteins (Figure 2). Since the ν_{CO} value is recognized as a sensitive index for the ρ_{Fe} (Scheme 1B),[2] the plots in Figure 2 confirmed a close relationship between the ρ_{Fe} and the resonance hybrid of the Fe-O_2 fragment (Scheme 1A), which underlays the electronic control of the heme Fe reactivity.

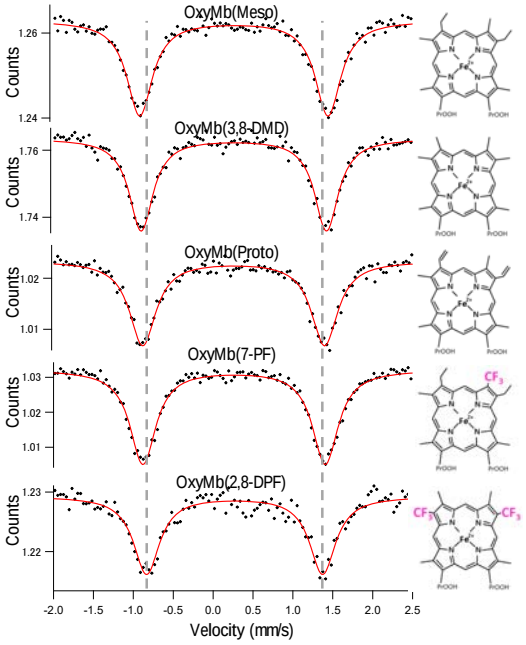

Figure 1. Mössbauer spectra of oxyMbs reconstituted with ^{57}Fe-labeled native and chemically-modified heme cofactors at 6 K.

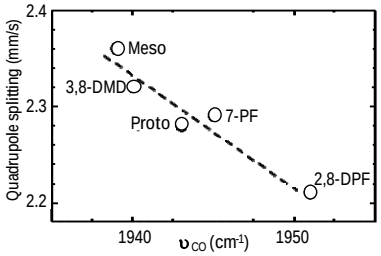

Figure 2. Plots of the quadrupole splittings against the ν_{CO} values of the proteins.

REFERENCES:

[1] T. Shibata, D. Matsumoto, R. Nishimura, H. Tai, A. Matsuoka, S. Nagao, T Matsuo, S. Hirota, K. Imai, S. Neya, S. Suzuki, and Y. Yamamoto, *Inorg. Chem.*, **51**, (2012) 11955–11960.

[2] R. Nishimura, T. Shibata, H. Tai, I. Ishigami, T. Ogura, S. Nagao, T. Matsuo, S. Hirota, K. Imai, S. Neya, A. Suzuki, and Y. Yamamoto, *Inorg. Chem.*, **52**, (2013) 3349-3355.

CO6-16 Potential of Boron Neutron Capture Therapy (BNCT) for Metastatic Bone: Study with Human Breast Cancer-bearing Animal Model

T. Fujimoto, T. Andoh[1], R. Satani[1], M. Suzuki[2], Y. Sakurai[2], T. Takata[2], H. Tanaka[2] and H. Ichikawa[2]

Hyogo Cancer Center,
Department of Orthopedic Surgery
[1]*Faculty of Pharmaceutical Sciences and Cooperative Research Center of Life Sciences,*
Kobe Gakuin University
[2]*Institute for Integrated Radiation and Nuclear Science, Kyoto University*

INTRODUCTION: In recent years, advances in chemotherapy for the treatment of cancer has markedly improved the prognosis of cancer patients. On the other hand, a remarkable increase in the number of cases of metastatic bone cancer has been evident, necessitating the introduction of new methods for treatment of the disease. Bone is vital/essential for supporting the body, in particular when cancer metastasizing to limb bones induces pathological fractures, a drastic decrease in the activity of daily life (ADL) and worsens the quality of life (QOL). Therefore, when metastasis to limb bones reaches the stage of impending fracture, preventive osteosynthesis is carried out for preventing pathological fractures. Nonetheless, since this procedure does not remove the tumor, postoperative radiotherapy for the entire surgical site is requisite for about 2 months — a very invasive procedure, especially for end-stage cancer patients. Therefore, in this study, a newly created human breast cancer-bearing animal model was used to investigate whether BNCT, a minimally invasive and non-surgical procedure, can control bone metastases.

EXPERIMENTS: All animal experiments were carried out according to the regulations of the Animal Care and Use Committee.
(1) Tumor cell line: Human breast cancer cell line MDA-MB-231-luc was cultured in Leibovitz's L-15 with fetal bovine serum in a 5% CO2 humidified incubator at 37˚C.
(2) Producing bone metastasis in the human breast cancer-bearing animal model: MDA-MB-231-luc cells suspended in Matrigel® were transplanted into the tibia of the left hind leg of nude mice. Eight weeks thereafter, the formation of a tumor was confirmed by micro-CT scans.
(3) BNCT in vivo: The mice were divided into two groups.
Under anesthesia and through the femoral vein, the BNCT group and the control group were administered BPA-Fr (24 mg 10B/kg) and saline, respectively. After an interval of 90 min, and according to the biodistribution data of 10B in this animal model as previously described [1], thermal neutrons (1 MW) were irradiated for 60 min onto the left hind leg of the mice under anesthesia in the heavy water facility at KURRI. Nine weeks after the irradiation, the left hind leg of the animals was observed by imaging techniques. The mice were then terminated and tissue specimens collected immediately and stained with hematoxylin-eosin (HE) for histological analysis.

RESULTS: Imaging studies before BNCT disclosed two type of bone metastasis in the femur: 1) a pathological fracture had already occurred [Fig. 1A] and 2) the tumor was present in the intact femur. The physical dose (Gy) absorbed by the tumor and skin of the BNCT group was 5.0 Gy and 2.0 Gy, respectively. Nine weeks after the irradiation, no abnormality was macroscopically observed in the epidermis at the irradiated site. Imaging analysis revealed tumor shrinkage in metastatic foci in the type-2 BNCT group. Conversely, pathological studies of the type-1 BNCT group disclosed an increase in the tumor mass at the irradiation site [Fig. 1B]. No shrinkage of the tumor mass was observed in the control group. The results suggested that when a pathological fracture occurs, the tumor diffuses to the surroundings of the fracture site through blood, and the tumor is less likely to take up boron at BPA administration; also, that BNCT has no effect on pathological fractures. Therefore, the administration of a boron preparation including BSH may be needed for accumulation in the surrounding tumor cells when a pathological fracture is present.

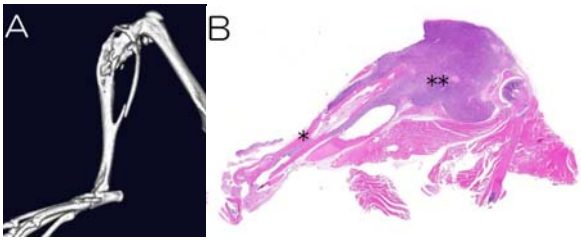

[Fig. 1] A; 3D-CT image of the pathological fracture of left tibia 5days after BNCT.
B; HE staining of left side of mouse model. The pathological study demonstrated the tumor mass extending from the intramedullary to the surface of the tibia. *: cortex of tibia, **: tumor.

REFERENCE:

[1] Biodistribution of p-borono-L-phenylalanine in human breast cancer-bearing bone metastasis animal model for BNCT. T. Fujimoto *et al*. KURRI Progress Report 2016, PR6-2.

CO6-17 Preparation of F1Fo-ATP Synthase as a Whole Body Complex from Bovine Heart for Structural Analysis by Cryo-electron Microscopy and X-ray Crystallography

C. Jiko, A. Uehara, C. Gerle[1], and Y. Morimoto

Institute for Integrated Radiation and Nuclear Science, Kyoto University

[1]*Institute for Protein Research, Osaka University*

INTRODUCTION: The mitochondrial F type ATP synthase functions as a mammalian energy transducer for the homeostasis of the living cell. It not only produces ATP to over 90 % during respiration (Boyer, An-nu.Rev.Biochem.,1997), but also plays an important role in the architecture of the inner membrane (Davies et al., PNAS, 2012) and apoptosis cascade (Giorgio et al., PNAS, 2013). In addition, lack of the enzyme may lead to deseases in neuropathology and metabolic disorders. However, to date neither the reaction mechanism of the ATP nor rotational motion of the enzyme is understood in detail, since the tertiary structure of the enzyme has not been clarified at atomic resolution.

Structural analyses of the F-ATP synthase have been going on for over 50 years and lead to two Nobel prizes until now, but they are restricted to the soluble F1 domain and subcomplexes by X-ray crystal structure analysis (Walker, Biochem. Soc. Tran., 2013). There is no report of an intact F-ATP synthase complex. On the other hand, cryo-electron microscopy (cryo-EM) has become a powerful tool for a structure analysis of large macromolecular complexes and can be used as a checking method of purified samples for crystallographic studies. It is essential that a highly homogeneity of the samples should be led to a suitable crystal even a huge and multi-domain complex, an external form and popu-lation from them should be verified before set-up crystallization and function analyses. We have prepared the F1Fo ATP synthase complex as a whole body and a dimer forming from bovine heart, and crystallized them. A selection of detergents at a preparation step and application of the GraDeR method for cryo-EM are very useful for the future research. Here, we report a preparation steps of F1Fo ATP synthase in this institute and show TEM images from the prepared samples in order to determine purities of them by use of Mo- or Uranium acetate (Ac-U)- treatment.

EXPERIMENTS: Bovine heart was obtained just after slaughter at Nishinomiya field, and their mitochondria was isolated by the red-green separation process under ultracentrifugation steps with use of the buffer, 40mM HEPES-Na(pH7.4). A density gradient by ultracentrifugation supplied a red component containing the enzymes (Fig.1).

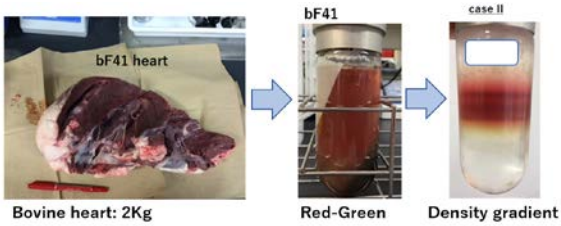

Fig.1 Preparation step from bovine heart to enzyme component

TEM images of the prepared enzyme were obtained by the Hitachi HT7800 operated by 80kV, 10μA at the Institute for Protein Research, Osaka University. Ac-U solution after re-batch uranyl reagent was prepared in the restricted hot-lab area in our institute under the conductor and nuclear guidelines.

RESULTS and DISCUSSION: TEM images (Fig.2) under Ac-U stain clearly shows enzyme forms monomer, dimer or tetramer with high contrast, other Mo-stain shows poorly formation of the enzyme. The later could not lead us to decide how preparation steps are suitable for cryo-EM and crystallization.

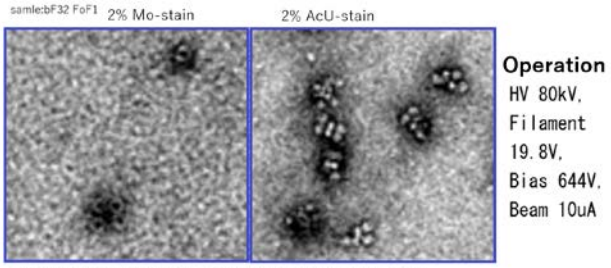

Fig.2 Typical TEM images of the whole enzyme, left: Mo stain, right: uranyl acetate staining.

As seen in the micrograph of the negatively stained purified F1Fo-ATP synthase complexes, the dimeric shape of the complex is well preserved. In addition, a monodisperse distribution, crucial for both 3D crystallization and cryo-EM, is observed.